Title
Probing the impact of gamma-irradiation on the metabolic state of neural stem and precursor cells using dual-wavelength intrinsic signal two-photon excited fluorescence

Journal
J. Innov. Optical Health Sci., 4

Authors
Limoli, CL
Krasieva, TB
Giedzinski, E
et al.

Publication Date
2011

Published in final edited form as:
J Innov Opt Health Sci. 2011 July 1; 4(3): 289–300. doi:10.1142/S1793545811001629.

PROBING THE IMPACT OF GAMMA-IRRADIATION ON THE METABOLIC STATE OF NEURAL STEM AND PRECURSOR CELLS USING DUAL-WAVELENGTH INTRINSIC SIGNAL TWO-PHOTON EXCITED FLUORESCENCE

TATIANA B. KRASIEVA[*,‡], **ERICH GIEDZINSKI**[†,§], **KATHERINE TRAN**[†,¶], **MARY LAN**[†,‖], **CHARLES L. LIMOLI**[†,**], and **BRUCE J. TROMBERG**[*,††]

[*]Laser Microbeam and Medical Program, Beckman Laser Institute, University of California, Irvine, 1002 Health Sciences Road East, Irvine, CA 92612, USA

[†]Department of Radiation Oncology, University of California, Irvine, California 92697, USA

Abstract

Two-photon excited fluorescence (TPEF) spectroscopy and imaging were used to investigate the effects of gamma-irradiation on neural stem and precursor cells (NSPCs). While the observed signal from reduced nicotinamide adenine dinucleotide (NADH) was localized to the mitochondria, the signal typically associated with oxidized flavoproteins (Fp) was distributed diffusely throughout the cell. The measured TPEF emission and excitation spectra were similar to the established spectra of NAD(P)H and Fp. Fp fluorescence intensity was markedly increased by addition of the electron transport chain (ETC) modulator menadione to the medium, along with a concomitant decrease in the NAD(P)H signal. Three-dimensional (3D) neurospheres were imaged to obtain the cellular metabolic index (CMI), calculated as the ratio of Fp to NAD(P)H fluorescence intensity. Radiation effects were found to differ between low-dose (≤ 50 cGy) and high-dose (≥ 50 cGy) exposures. Low-dose irradiation caused a marked drop in CMI values accompanied by increased cellular proliferation. At higher doses, both NAD(P)H and Fp signals increased, leading to an overall elevation in CMI values. These findings underscore the complex relationship between radiation dose, metabolic state, and proliferation status in NSPCs and highlight the ability of TPEF spectroscopy and imaging to characterize metabolism in 3D spheroids.

Keywords

Multiphoton microscopy; cellular metabolic index; gamma radiation; brain tumors; NAD(P)H; flavoproteins

[††]Corresponding author: bjtrombe@uci.edu.
[‡]tkrasiev@uci.edu
[§]egiedzin@uci.edu
[¶]katherit@uci.edu
[‖]lmlan@uci.edu
[**]climoli@uci.edu

1. Introduction

Cranial irradiation remains a frontline treatment for a large number of patients with primary or metastatic tumors in the brain. In many of these patients, particularly children, the likelihood of developing radiation-induced cognitive impairments is quite high.[1–3] Significant data have now come to light that suggest a compelling link between the radiation-induced depletion and/or damage of neural stem and precursor cells (NSPC) and the onset of cognitive dysfunction. Additional data have also linked changes in the function of these critical cells to alterations in oxidative and metabolic state following irradiation.[4] The rationale for undertaking the current multiphoton fluorescence microscopy and spectroscopy studies was aimed at dissecting further the mechanisms that underlie radiation-induced metabolic changes in NSPCs.

Radiation-induced cognitive impairment manifests after doses that are relatively lower than those typically required to produce overt tissue damage and often includes hippocampus-dependent functions involving learning, memory, and spatial information processing.[4–6] It is particularly noteworthy that the hippocampus is an active site of proliferation in the brain, in which multipotent stem/precursors regenerate and produce cells that migrate away to generate glia or neurons, defining the process referred to as neurogenesis.[7,8] The production of new neurons from the neural stem cell compartments via neurogenesis occurs throughout the lifetime of an organism and may well define the significance of these multipotent cells in the brain. Damaging agents such as ionizing radiation and chemotherapeutic drugs or adverse conditions such as oxidative stress, aging, or disease have the potential to deplete stem cell pools and inhibit neurogenesis, thereby promoting the severity and hastening the onset of cognitive decline.

Previous work has demonstrated that the response of multiple primary (rodent and human) NSPC to various radiation types (X-rays, protons, and heavy ions) involves an acute and persistent oxidative stress that can last for months.[9–13] This oxidative stress significantly alters proliferation, radiosensitivity, mitochondrial function, and differentiation. As a result, radiation-induced oxidative stress appears to be a biochemical mechanism that can influence a wide range of functions critical to neural precursor cell function and central nervous system (CNS) health.

Details regarding the nature of radiation-induced oxidative stress have become increasingly important, as the response of neural stem and precursor cells to different reactive oxygen species (ROS) and reactive nitrogen species (RNS) can vary.[4,14] The reactivity of specific ROS and RNS and their respective sites of production also impact intracellular signaling and damage profiles. As the hub of cellular energy production, mitochondria are a principle source of proxidant ROS in cells, owing to leaky electron transport through the chain of protein complexes supporting oxidative phosphorylation.[15–17] Non-mitochondrial sources (NADPH oxidases, peroxisomes) of reactive species also contribute to the oxidative burden in cells and can impact redox homeostasis and decisions of NSPC to proliferate or differentiate.[18,19] Given the importance of radiation-induced oxidative stress to the overall physiologic function of neural stem and precursor cells, two-photon microscopy and spectroscopy were employed to understand further the sensitivity of NSPC to changes in redox state.

The use of optical methods for noninvasive monitoring of cellular respiration, based on fluorescence properties of reduced pyridine nucleotides (NADH and NADPH, hereafter NAD(P)H) and/or oxidized Fp was first described by Britton Chance more than 50 years ago.[20,21] The fluorescence signals of Fp and NAD(P)H can be used for characterizing the cellular metabolism due to their prominence in the mitochondrial respiratory electron

transfer chain (ETC) and the fact that the two co-enzymes are near redox equilibrium.[22] Thus the oxidation/reduction ratio of these two components varies inversely. For this purpose, a ratio of fluorescence intensity signals can be expressed as (NAD (P)H/Fp, Fp/NAD(P)H, Fp/(Fp + NAD(P)H), or NAD(P)H/(NAD(P)H + Fp), and is commonly referred to as "redox ratio," "redox index" or "cellular metabolic index" (CMI). It is used as an indicator of metabolic activity that is proportional to mitochondrial cellular respiration.

Two-photon excited fluorescence (TPEF) is a particularly powerful approach for imaging CMI in single cells. Because it employs near-infrared (NIR) sources, single- or dual-wavelength TPEF can be used to rapidly form high-resolution redox state images in thick (~200–300 μm) tissues with minimal photodamage. Such an approach has been used recently to probe the metabolic mechanisms of pancreatic islet pyruvate responses,[23] the metabolic state of hair cells in cochlear preparations,[24] the metabolism of fibroblasts in human dermis,[25] epithelial cells and chondrocytes in mouse bronchial tissue,[26] oxidative stress in retinal epithelial cells,[27] acute myocardial injury in animal models,[28] and as method to gauge the response of photodynamic therapy and melanoma metastatic potential.[29–31] In stem cell research, redox fluorometry has been applied to discriminate between processes of self-renewal or differentiation.[32,33]

In this work we explore the potential of using TPEF microscopy techniques for monitoring radiation effects on pluripotent neural cells *in vitro*, unperturbed by any additional enzymatic or mechanical processing. Here we report our efforts to establish optimized imaging protocols for CMI measurements of multipotent neural stem cells cultured as three-dimensional (3D) neurospheres and to elucidate the intracellular source of radioresponsive fluorescence signals.

2. Materials and Methods

2.1. Growth and irradiation of neural stem and precursor cells

NSPCs were isolated from hippocampus of post-natal mice and grown in culture under serum-free conditions as neurospheres. Neurospheres were dissociated twice weekly into single cells suspensions and replated for growth and sphere formation in DME/F12 (Invitrogen), 0.4% bovine serum albumin (Sigma, St. Louis, MO, USA), 0.76 units/ml heparin (Sigma), 200 ng/ml epidermal growth factor (EGF, Biomedical Technologies, Stoughton, MA, USA), and 40 ng/ml fibroblast growth factor (FGF, Peprotech, Rocky Hills, NJ, USA). Under these conditions, the cells routinely exhibit doubling times on the order of 24 h.[4] One day prior to microscopic interrogation, single cells or well-formed neurospheres were plated on matrigel-coated chambered slides fitted with thin glass coverslips for TPEF measurements. Once anchored (~2 h), the slides containing cells and/or neurospheres were subject to γ-irradiation using a ^{137}Cs irradiator (J.L. Shepard and Associates Mark I) at a dose rate of 1.17 Gy/min over a dose range of 0 to 5 Gy. Following irradiation, cells were returned to humidified incubators (37°C, 5% CO_2) until imaging the following day. For those cultures subjected to ETC modulators, drugs were added after initial two-photon imaging. Vitamin K_3 (Menadione, Sigma) was used at 10–20 mM, while the complex III inhibitor (Antimycin A, Sigma) was used at 1–5 mM.

For uniformity of measurements and to minimize potential metabolic stress associated with limited oxygen diffusion across larger sized spheres, 3D neurospheres of relatively similar dimensions (75 ± 25 μm diameter, 285 ± 45 cells/neurosphere) were imaged.[4]

2.2. Proliferation assays

For measurements of cellular proliferation, irradiated neurospheres were plated at 10,000 cells/well (24-well plates) and allowed to proliferate for up to 4 days. Survival of irradiated

cells was determined by the quantification of DNA based on a SYBR green fluorescence. On the day of harvest, cells were washed with PBS and incubated at −80°C overnight to facilitate cell lysis. On the subsequent day, cells were lysed using M-PER (Mammalian Protein Extraction Reagent, Thermo Scientific) containing 2.5 × SYBR Green I (Invitrogen). SYBR Green I was excited at 497 nm and the fluorescence was measured at 520 nm on a microplate reader (SynergyMx, BioTek, Vermont, USA) and compared to a standard curve to yield actual cell counts.

2.3. Imaging and instrumentation

All imaging and spectral experiments were performed on Zeiss LSM 510 NLO microscopy system with Chameleon-Ultra (Coherent, Inc.) femtosecond-pulsed laser tunable from 690 to 1040 nm as a source of excitation. Laser scanning did not induce any visible damage to the cells or noticeable bleaching of the sample. Detector (Hamamatsu PMTs) settings were chosen to keep the signal intensity on a linear part of the response curve.

Neural precursor cells were imaged as live 3D neurospheres that were anchored to the bottom of the imaging chamber as described above. Imaging dishes were kept at 34°C throughout all the imaging experiments in a temperature-controlled chamber (Warner Instrument Corporation, Hamden, CT, USA).

In order to minimize scattering effects, all imaging was performed at a distance of approximately 15–20 μm above the coverslip surface (second cellular layer in spheroids).

Spheroids were imaged sequentially with excitation at 720 nm, emission isolated with a band pass filter 420–475 nm for NAD(P)H (blue channel), and excitation 900 nm, emission 500–550 nm for Fp (green channel). Images were routinely merged to confirm that the imaging planes of both acquisitions were the same. The objective used in all experiments was a Zeiss Apochromat (40X water immersion, long working distance, numerical aperture 0.8) with excellent light transmittance properties from UV and up to 1100 nm. All images were 225 × 225 μm^2.

The average intensity of measured blue and green channel signals for non-irradiated samples was set to be close to unity. All data were collected in 12-bit (maximum allowable by the instrument) mode.

All spectral measurements were supported by the 32-detector Meta channel of the LSM510 system. Excitation power was measured and normalized (by square dependence between excitation power and fluorescence intensity) to 50 mW at the sample for the excitation spectra measurements.

2.4. Quantification of fluorescence signal for statistical analyses

All images were converted from Zeiss LSM .lsm format to 12-bit TIFF and exported to specialized quantitative imaging software program IPLab Spectrum (Scanalytics, BD Biosciences-Bioimaging, San Jose, CA, USA). Values for CMI were calculated as the mean fluorescent ratios of the Fp over NAD(P)H channels (i.e. green/blue) for the total cross sectional areas of each spheroid.

The fluorescence signal for the flavoproteins was measured as a mean value of each individual cluster. Some of the spheroids contained a few (1–3) cells with abnormally high fluorescence intensity (2.5–3 times over mean levels/values). Those cells were excluded from the count.

Each data point represents five independent fields of view, containing one or two individual spheroids (representing a minimum of ~1400 ± 200 total cells analyzed). All data were corrected for background noise measured in each individual image separately.

3. Results

Initial images of spheroids excited at 800 nm showed that the blue NAD(P)H fluorescence signal arose mainly from the mitochondria as expected, while the green Fp fluorescence signal was surprisingly bright and diffuse throughout the whole cell (Fig. 1). Prior work has shown, that the green fluorescence emitted in this spectral region was mainly FPs and was relatively weak and almost exclusively associated with the mitochondria.[34–36] To further verify the origin of the diffuse signal, and minimize fluorescent overlap between channels, sequential excitation at 720 nm for NAD(P)H (blue) and 900 nm for Fp (green) eliminated spectral crosstalk and confirmed the diffuse cytoplasmic distribution of green fluorescence. Strong non-mitochondrial–bound Fp fluorescence is not unique however, as cells have been shown to display bright, diffuse Fp derived fluorescence.[37,38] These studies suggested that multiple sources of oxidized Fp occur within the cell, some of which are not necessarily associated with the mitochondrial ETC proteins.

To gain insight into the origin of the fluorescence signals under study, we measured excitation and emission fluorescence spectra from various sub-cellular regions (mitochondrial, cytoplasmic, nuclear) in the nonirradiated spheroids. Both excitation and emission spectra of NAD(P)H were very similar to those previously reported in the literature[34,39] with an excitation maximum at 720 nm and an emission peak at 460–475 nm (Fig. 2). The two-photon fluorescence emission spectra (Fig. 3) excited at 900 nm were similar to the spectra of two different oxidized flavoproteins reported in Ref. 34. The FAD maximum is at 540 nm. The FAD of alpha-lipoamide dehydrogenase (LipDH)[40] has emission maximum at 520 nm and considered to be a main source of flavin fluorescence in mitochondria and is in equilibrium with the mitochondrial NAD+/NADH couple. This corresponds well with the relatively higher intensity of the 520-nm peak measured for mitochondrial regions in the cells with lower or negligible diffuse green fluorescence (Fig. 3).[41] The diffuse signal had a relatively higher intensity of the FAD+ (540 nm max). The excitation spectra showed the expected peak at 900 nm that is typically ascribed to FAD and additional peak blue-shifted to 860 nm. Spectral data reported in Ref. 34 also exhibited a local maximum at about 850 nm for LipDH.

To investigate further the possibility that the green fluorescent signal might be derived from an oxidized Fp moiety, possibly active in ETC respiration, we chose to chemically modulate specific complexes involved in mitochondrial ETC. Addition of menadione (MEN, Vitamin K_3), can stimulate electron transfer within the inner membranes of the mitochondria,[42] which can produce a significant and rapid increase in Fp and decrease in NAD(P)H fluorescence intensity respectively (Figs. 4 and 5). The increase in Fp fluorescence was associated with both punctuate mitochondrial signals and more diffuse cytoplasmic/nuclear localized signals. Addition of the complex III inhibitor antimycin A (AntA) caused an opposite and less significant effect, whereby the mitochondrial-associated NADH signal intensity increased in the relative absence of a decreased signal from oxidized Fp (Figs. 4 and 5). Addition of the solvent ethyl alcohol alone as a negative control did not cause any statistically significant changes in fluorescence intensity of either signal (Fig. 5).

3.1. Radioresponsive effects

In order to quantify the effects of irradiation on the cellular metabolic activity levels, we measured relative changes in NAD(P)H and Fp fluorescence intensity and calculated CMI as the ratio of Fp/NAD(P)H signals normalized to sham-irradiated controls set to unity.

The fluorescence of NAD(P)H showed a normal distribution within neurospheres (data not shown). Cell-to-cell variations in the Fp signal were very significant (Figs. 1 and 4) and did not show an overt correlation with the NAD(P)H signal intensity between individual cells. All irradiated neurospheres contained a certain fraction of cells exhibiting Fp fluorescence intensity 2.5–3 times brighter than the mean signal intensity of the entire neurosphere. These cells were excluded from the measurements (see Sec. 2).

NAD(P)H signal intensity showed a dose-response, increasing linearly over the dose range analyzed [Fig. 6(a)]. At lower doses (≤50 cGy) the Fp signal intensity was found to drop, an effect that was reversed as the total dose was increased up to 5 Gy [Fig. 6(b)]. Based on the foregoing measurements, the CMI showed a corresponding sharp decrease in the low dose regions; the NAD(P)H and Fp signals changed in the opposite directions [Fig. 6(c)]. At higher doses the CMI increased, reflecting the rise in both signals, albeit at different rates [Fig. 6(c)].

To explore the functional significance of these metabolic signals, we analyzed the impact of low-dose irradiation on cellular proliferation. Neurospheres subjected to low-dose exposure (≤30 cGy) exhibited significantly increased ($p \leq 0.05$, ANOVA) proliferation compared to sham-irradiated controls (Fig. 7). Low-dose exposure to 10 or 30 cGy, yielded increased proliferation of 1.1- and 1.3-fold respectively, compared to sham-irradiated controls.

4. Discussion

Past work has shown that radiation-induced oxidative stress in multipotent neural precursor cells is both dose-responsive and persistent.[9,10,13] The resultant redox changes can alter important physiologic parameters such as proliferation, differentiation, and radiosensitivity. The ability to analyze living cells under minimal perturbation using two-photon excitation of intrinsic fluorophores is a powerful approach for monitoring the redox status in cells. In this study we define CMI as a ratio of oxidized Fp/reduced NAD(P)H due to a direct correlation between CMI values and the cellular metabolic levels. Using this marker of redox state, CMI has been used to describe a number of distinct respiratory states.[22,30] Under physiological oxygen availability (~3–5%O_2), low levels of oxidative metabolism manifest as high NADH and low Fp signal intensities, (i.e., low CMI values). Higher levels of oxidative metabolism are accompanied by higher values of oxidized Fp and lower levels of reduced NAD(P)H. While absolute CMI values are difficult to use for comparisons between multiple experiments conducted over time, relative changes normalized to unirradiated controls run in parallel, provide the means for quantifying significant changes in the cellular metabolic state caused by a variety of factors.

How cells respond specifically to irradiation to increase oxidative stress has been a topic receiving significant attention over recent years. Past work has shown that the mitochondria and their electron transporting activities contribute to a certain fraction of radiation-induced oxidative stress.[10,13,43] Other work has also identified the NAD(P)H oxidases as a sources of pro-oxidants in irradiated cells.[18,19,44] For example, NAD(P)H oxidase consists of several components and one of them, p91-phox, is a flavoprotein.[37]

In this light, the observations reported here that low-dose irradiation (≤ 50 cGy) leads to a decrease in the oxidized Fp signal and an increase in the NAD(P)H signal are significant. The resultant drop in CMI as measured by two-photon microscopy may reflect a general decrease in the metabolic activity of cells subjected to low-dose irradiation [Fig. 6(c)], possibly in an effort to bolster energy reserves for the synthesis of macromolecular precursors.[45,46] Diminishing mitochondrial oxidative metabolism to adequately support the generation of protein, nucleic acid and lipid precursors needed for proliferation may be a prime consequence of mild irradiation stress. In support of this idea, cells subjected to low-

dose irradiation were found to respond by elevating proliferation (Fig. 7). These low-dose effects clearly differ from higher dose effects, typically observed under more clinically relevant dosing paradigms.

Precisely how low-dose irradiation impacts the metabolic state of cells is uncertain, but past reports documenting “protective” radiation-induced adaptive responses may provide clues. Changes in oxidative stress caused by low-dose exposure can elicit alternative gene expression that engage prosurvival pathways that can be linked to the energy demands of cells.[47,48] Adaptive responses have been documented for a number of cell types and endpoints and are generally found to promote DNA repair and survival.[49,50] In the CNS, elevations in superoxide levels may account for the neuroprotective effects in irradiated cells and animals deficient in superoxide dismutase.[51,52] The link between radiation-induced alterations in mitochondrial respiration may provide a mechanistic basis for the changes in CMI with radiation exposure noted above. For glial precursor cells[32] and mesenchymal stem cells,[33] changes to the intracellular redox state have been shown to be critical to the balance between self-renewal or differentiation. Of interest in this regard were findings, showing that self-renewal was associated with a relatively reduced intracellular state (lower CMI), while differentiation was associated with an oxidized intracellular state (higher CMI). This result is consistent with the proliferative status of our neural precursor cultures and the observed drop in average CMI value found postirradiation (Figs. 6(c) and 7).

Further increases in radiation exposure (up to a maximum used dose of 5 Gy) caused a gradual increase in CMI values. However, at these higher doses, the increased oxidized Fp signal was not complimented by a decreased NAD(P)H signal, which would be an indication of elevated cellular respiration. The increase in both signals may be indicative of higher oxidative stress and early marker of apoptosis.[28,53] Matsui and co-authors reported an increase in diffuse FAD fluorescence in the cytoplasm of rat gastric mucosal epithelial cells injured by H_2O_2 according to the extent of injury”. Persistent oxidative stress may drive the need for reducing equivalents in the form of NADPH. Thus, it is conceivable that the elevated NAD(P)H signal is derived from a certain fraction of NADPH generated from the oxidative pentose phosphate cycle.[54,55]

The oxidized Fp signal exhibits significant heterogeneity within neurospheres, likely emanating from both the mitochondrial and nonmitochondrial compartments. A significant fraction of the non-redox responsive Fp signal (i.e., free flavins) may indicate that their oxidative state is not directly coupled to ETC.[23] The precise nature of this diffuse signal is more difficult to pinpoint, owing to the multiple cytoplasmic flavoproteins. In the case of FAD covalently bound to proteins and in a less restrictive, solvent accessible environment (cytoplasm, nucleus), fluorescence should be stronger due to minimal quenching compared to the mitochondrial environment. Possible candidates include the various isoforms of NADPH oxidase and nitric oxide synthase, all enzymes that have been shown to be radioresponsive.[18,56] Generation of superoxide by the NADPH oxidases could increase the yield of oxidized FAD, and evidence that irradiation increases superoxide levels from the mitochondria and NADPH oxidases has been found in neural stem cells, neural precursor cells, as well as other cell types.[10,13,18,43,44,56] One-electron reduction of oxidants generates ROS through redox cycling; the pro-oxidant MEN generates ROS via this pathway[57] with concomitant decreases in NAD(P)H. Significant decreases in NAD(P)H intensity, accompanied by increased oxidized F_Ps (Figs. 4 and 5), elicits significant increases in the CMI value. The MEN-induced production of ROS promotes apoptosis, which has been linked itself to increased oxidative stress.[28,29,58] Radiation has also been found to stimulate nitric oxide (NO) production in a similar spectrum of cell types,[19,56] and generation of NO could drive an increase in oxidized FAD.

There are two major sites along the respiratory chain that can generate ROS: one dependent upon the oxidation of the flavin mononucleotide from the NADH-dehydrogenase (complex I), the second dependent upon the auto-oxidation of the unstable ubisemiquinone (complex III).[59] Inhibition of complex III by AntA (blocker of ubisemiquinone) caused a small drop in CMI, mainly due to the increase in NAD(P)H (Figs. 4 and 5). Such a variation could be attributed to a difference between superoxide production and the activity of mitochondrial electron transport.

In summary, our two-photon microscopy studies have corroborated a number of past findings documenting changes in the redox state of irradiated cells. While the fluorescent signals measured may well represent contributions from several distinct molecules, it is clear that TPEF-measured CMI provides a useful gauge of metabolic activity in NSPCs and may provide a sensitive readout of low-dose radiation effects as they relate to altered metabolism.

Acknowledgments

This work was supported by U.S. Department of Energy, Grant No. DE-FG02-09ER64798 (CLL), National Aeronautics and Space Administration Grant No. NNX09AK25G (CLL) and American Cancer Society Grant No. RSG-00-036-04-CNE (CLL), National Institute of Health NIH LAMMP P41 Grant No. R01192 (BJT, TBK), National Cancer Institute 2P30CA62203 (BJT, TBK).

References

1. Abayomi OK. Pathogenesis of irradiation-induced cognitive dysfunction. Acta Oncol. 1996; 35(6): 659–663. [PubMed: 8938210]
2. Tofilon PJ, Fike JR. The radioresponse of the central nervous system: A dynamic process. Radiat Res. 2000; 153(4):357–370. [PubMed: 10798963]
3. Meyers CA, Brown PD. Role and relevance of neurocognitive assessment in clinical trials of patients with CNS tumors. J Clin Oncol. 2006; 24(8):1305–1309. [PubMed: 16525186]
4. Fike JR, Rosi S, Limoli CL. Neural precursor cells and central nervous system radiation sensitivity. Semin Radiat Oncol. 2009; 19(2):122–132. [PubMed: 19249650]
5. Clelland CD, Choi M, Romberg C, Clemenson GD Jr, Fragniere A, Tyers P, Jessberger S, Saksida LM, Barker RA, Gage FH, Bussey TJ. A functional role for adult hippocampal neurogenesis in spatial pattern separation. Science. 2009; 325(5937):210–213. [PubMed: 19590004]
6. Meyers CA, Geara F, Wong PF, Morrison WH. Neurocognitive effects of therapeutic irradiation for base of skull tumors. Int J Radiat Oncol Biol Phys. 2000; 46(1):51–55. [PubMed: 10656372]
7. Palmer TD, Takahashi J, Gage FH. The adult rat hippocampus contains primordial neural stem cells. Mol Cell Neurosci. 1997; 8(6):389–404. [PubMed: 9143557]
8. Gage FH. Mammalian neural stem cells. Science. 2000; 287(5457):1433–1438. [PubMed: 10688783]
9. Giedzinski E, Rola R, Fike JR, Limoli CL. Efficient production of reactive oxygen species in neural precursor cells after exposure to 250 MeV protons. Radiat Res. 2005; 164(4 Pt 2):540–544. [PubMed: 16187784]
10. Limoli C, Giedzinski E, Rola R, Otsuka S, Palmer T, Fike J. Radiation response of neural precursor cells: Linking cellular sensitivity to cell cycle checkpoints, apoptosis and oxidative stress. Radiat Res. 2004; 161:17–27. [PubMed: 14680400]
11. Limoli CL, Giedzinski E, Baure J, Rola R, Fike JR. Altered growth and radiosensitivity in neural precursor cells subjected to oxidative stress. Int J Radiat Biol. 2006; 82(9):640–647. [PubMed: 17050476]
12. Limoli CL, Giedzinski E, Baure J, Rola R, Fike JR. Redox changes induced in hippocampal precursor cells by heavy ion irradiation. Radiat Environ Biophys. 2007; 46(2):167–172. [PubMed: 17103219]

13. Acharya MM, Lan ML, Kan VH, Patel NH, Giedzinski E, Tseng BP, Limoli CL. Consequences of ionizing radiation-induced damage in human neural stem cells. Free Radic Biol Med. 2010; 49(2): 1846–1855. [PubMed: 20826207]
14. Fike JR, Rola R, Limoli CL. Radiation response of neural precursor cells. Neurosurg Clin North Am. 2007; 18(1):115.
15. Boveris A. Mitochondrial production of super-oxide radical and hydrogen peroxide. Adv Exp Med Biol. 1977; 78:67–82. [PubMed: 197811]
16. Boveris, A.; Cadenas, E. Production of superoxide radicals and hydrogen peroxide in mitochondria. In: Oberley, LW., editor. Superoxide Dismutase. Vol. II. CRC Press; Boca Raton, FL: p. 15-30.
17. Voet, D.; Voet, JG.; Pratt, CW. Fundamentals of Biochemistry. Vol. Chapter 17. John Wiley & Sons, Inc; 1999. Electron transport and oxidative phosphorylation; p. 492-525.
18. Collins-Underwood JR, Zhao W, Sharpe JG, Robbins ME. NADPH oxidase mediates radiation-induced oxidative stress in rat brain microvascular endothelial cells. Free Radic Biol Med. 2008; 45(6):929–938. [PubMed: 18640264]
19. Wang Y, Liu L, Pazhanisamy SK, Li H, Meng A, Zhou D. Total body irradiation causes residual bone marrow injury by induction of persistent oxidative stress in murine hematopoietic stem cells. Free Radic Biol Med. 2010; 48(2):348–356. [PubMed: 19925862]
20. Chance B, Baltscheffsky H. Respiratory enzymes in oxidative phosphorylation. J Biol Chem. 1958; 233(3):736–739. [PubMed: 13575447]
21. Chance B, Cohen P, Jobsis G, Schoener B. Intracellular oxidation-reduction states *in vivo*. Science. 1962; 137:499–508. [PubMed: 13878016]
22. Chance B, Schoener B, Oshino R, Itshak F, Nakase Y. Oxidation-reduction ratio studies of mitochondria in freeze-trapped samples. NADH and flavoprotein fluorescence signals. J Biol Chem. 1979; 254(11):11.
23. Rocheleau JV, Steven HW, Piston DW. Quantitative NAD(P)H/flavoprotein auto-fluorescence imaging reveals metabolic mechanisms of pancreatic islet pyruvate response. J Biol Chem. 2004; 279(30):31780–31787. [PubMed: 15148320]
24. Tiede LM, Rocha-Sanchez SM, Hallworth R, Nichols MG, Beisel K. Determination of hair cell metabolic state in isolated cochlear preparations by two-photon microscopy. J Biomed Opt. 2007; 12(2):021004. [PubMed: 17477711]
25. Zhuo Shuangmu CJ, Jiang X, Cheng X, Xie S. Visualizing extracellular matrix and sensing fibroblasts metabolism in human dermis by nonlinear spectral imaging. Skin Res Technol. 2007; 13(4): 406–411. [PubMed: 17908192]
26. Zhuo S, Chen J, Yu B, Jiang X, Luo T, Liu Q, Chen R, Xie S. Nonlinear optical microscopy of the bronchus. J Biomed Opt. 2008; 13(5):7.
27. del Marisol V, Cano JMR, Park CY, Gao X, Mori K, Chuck RS, Gehllach PL. Demonstration by redox fluorometry that sulforaphane protects retinal pigment epithelial cells against oxidative stress. Invest Ophthalmol Visual Sci. 2008; 49(6):2606–2612. [PubMed: 18515589]
28. Ranji M, Matsubara M, Leshnower BG, Hinmon RH, Jaggard DL, Chance B, Gorman RC, Gorman JH. Quantifying acute myocardial injury using ratiometric fluorometry. IEEE Transact Biomed Eng. 2009; 56(5):1556–1563.
29. Zhang Z, Blessington D, Li H, Busch TM, Glickson J, Luo Q, Chance B, Zheng G. Redox ratio of mitochondria as an indicator for the response of photodynamic therapy. J Biomed Opt. 2004; 9(4): 772–778. [PubMed: 15250765]
30. Li, LZJ.; Zhong, ZRT.; Moon, L.; Kim, EJ.; Qiao, H.; Pickup, S.; Hendrix, MJ.; Leeper, D.; Chance, B.; Glickson, JD. Predicting melanoma metastatic potential by optical and magnetic resonance imaging. In: Maguire, DJ.; Bruely, DF.; Harrison, DK., editors. Oxygen Transport to Tissue XXVIII. 2007. p. 67-78.
31. Li LZ, Zhou R, Xu HN, Moon L, Zhong T, Kim EJ, Qiao H, Reddy R, Leeper D, Chance B, Glicksona JD. Quantitative magnetic resonance and optical imaging biomarkers of melanoma metastatic potential. PNAS. 2009; 106(16):6608–6613. [PubMed: 19366661]

32. Smith J, Ladi E, Mayer-Proschel M, Noble M. Redox state is a central modulator of the balance between self-renewal and differentiation in a dividing glial precursor cell. PNAS. 2000; 97(18): 10032–10037. [PubMed: 10944195]
33. Reyes JMG, Fermanian S, Yang F, Zhou S-Y, Herretes S, Murphy DB, Elisseeff JH, Chuck RS. Metabolic changes in mesenchymal stem cells in osteogenic medium measured by autofluorescence spectroscopy. Stem Cells. 2006; 24:1213–1217. [PubMed: 16439616]
34. Huang S, Heikal AA, Webb WW. Two-photon fluorescence spectroscopy and microscopy of NAD (P)H and flavoprotein. Biophys J. 2002; 82(5):2811–2825. [PubMed: 11964266]
35. Scholz R, Thurman RG, Williamson JR, Chance B, Bucher T. Flavin and pyridine nucleotide oxidation-reduction changes in perfused rat liver. I. Anoxia and subcellular localization of fluorescent flavoproteins. J Biol Chem. 1969; 244(9):2317–2324. [PubMed: 4306507]
36. Koke JR, Wylie W, Wills M. Sensitivity of flavoprotein fluorescence to oxidative state in single isolated heart cells. Cytobios. 1981; 32(127–128):139–145. [PubMed: 7347273]
37. Kindzelskii A, Petty HR. Fluorescence spectroscopic detection of mitochondrial flavoprotein redox oscillations and transient reduction of the NADPH oxidase-associated flavoprotein in leukocytes. Eur Biophys J. 2004; 33(4):291–299. [PubMed: 14574524]
38. Chorvat D Jr, Kirchnerova J, Cagalinec M, Smolka J, Mateasik A, Chorvatova A. Spectral unmixing of flavin autofluorescence components in cardiac myocytes. Biophys J. 2005; 89(6):L55–L57. [PubMed: 16227502]
39. Patterson GH, Knobel SM, Arkhammar P, Thastrup O, Piston DW. Separation of the glucose-stimulated cytoplasmic and mitochondrial NAD(P) H responses in pancreatic islet b cells. Proc Natl Acad Sci. 2000; 97(10):5.
40. Shiino, A.; Matsuda, M.; Chance, B. Methods in Enzymology. Vol. 352. Elsevier; 2002. Three-dimensional redox imaging of frozen-quenched brain and other organs; p. 8
41. Kunz WS, Kunz W. Contribution of different enzymes to flavoprotein fluorescence of isolated rat liver mitochondria. Biochim Biophys Acta. 1985; 841(3):237–246. [PubMed: 4027266]
42. Shneyvays V, Leshem D, Shmist Y, Zinman T, Shainberg A. Effects of menadione and its derivative on cultured cardiomyocytes with mitochondrial disorders. J Mol Cell Cardiol. 2005; 39(1):149–158. [PubMed: 15893762]
43. Leach JK, Van Tuyle G, Lin PS, Schmidt-Ullrich R, Mikkelsen RB. Ionizing radiation-induced, mitochondria-dependent generation of reactive oxygen/nitrogen. Cancer Res. 2001; 61(10):3894–3901. [PubMed: 11358802]
44. Venkatachalam P, de Toledo SM, Pandey BN, Tephly LA, Carter AB, Little JB, Spitz DR, Azzam EI. Regulation of normal cell cycle progression by flavin-containing oxidases. Oncogene. 2008; 27(1):20–31. [PubMed: 17637756]
45. Vander Heiden MG, Cantley LC, Thompson CB. Understanding the Warburg effect: The metabolic requirements of cell proliferation. Science. 2009; 324(5930):1029–1033. [PubMed: 19460998]
46. Denko NC. Hypoxia, HIF1 and glucose metabolism in the solid tumour. Nat Rev Cancer. 2008; 8(9):705–713. [PubMed: 19143055]
47. Spitz DR, Sim JE, Ridnour LA, Galoforo SS, Lee YJ. Glucose deprivation-induced oxidative stress in human tumor cells. A fundamental defect in metabolism? Ann N Y Acad Sci. 2000; 899:349–362. [PubMed: 10863552]
48. Spitz DR, Azzam EI, Li JJ, Gius D. Metabolic oxidation/reduction reactions and cellular responses to ionizing radiation: A unifying concept in stress response biology. Cancer Metastasis Rev. 2004; 23(3–4):311–322. [PubMed: 15197331]
49. Azzam EI, de Toledo SM, Little JB. Stress signaling from irradiated to non-irradiated cells. Curr Cancer Drug Targets. 2004; 4(1):53–64. [PubMed: 14965267]
50. de Toledo SM, Asaad N, Venkatachalam P, Li L, Howell RW, Spitz DR, Azzam EI. Adaptive responses to low-doseslow-dose-rate gamma rays in normal human fibroblasts: The role of growth architecture and oxidative metabolism. Radiat Res. 2006; 166(6):849–857. [PubMed: 17149977]
51. Fishman K, Baure J, Zou Y, Huang TT, Andres-Mach M, Rola R, Suarez T, Acharya M, Limoli CL, Lamborn KR, Fike JR. Radiation-induced reductions in neurogenesis are ameliorated in mice

deficient in CuZnSOD or MnSOD. Free Radic Biol Med. 2009; 47(10):1459–1467. [PubMed: 19703553]

52. Rola R, Zou Y, Huang TT, Fishman K, Baure J, Rosi S, Milliken H, Limoli CL, Fike JR. Lack of extracellular superoxide dismutase (EC-SOD) in the microenvironment impacts radiation-induced changes in neurogenesis. Free Radic Biol Med. 2007; 42(8):1133–1145. discussion 1131–112. [PubMed: 17382195]
53. Matsui H, Murata Y, Hirano K-I, Sasaki T, Shiba R, Muto H, Ono T. Hydrogen peroxid-induced cellular injury is associated with increase in endogenous fluorescence from rat gastric mucosal epithelial cell culture: A new method for detecting oxidative cellular onjury by fluorescence measurement. J Gastroenterol. 1998; 33:8.
54. Tuttle SW, Maity A, Oprysko PR, Kachur AV, Ayene IS, Biaglow JE, Koch CJ. Detection of reactive oxygen species via endogenous oxidative pentose phosphate cycle activity in response to oxygen concentration: Implications for the mechanism of HIF-1alpha stabilization under moderate hypoxia. J Biol Chem. 2007; 282(51):36790–36796. [PubMed: 17666400]
55. Tuttle S, Stamato T, Perez ML, Biaglow J. Glucose-6-phosphate dehydrogenase and the oxidative pentose phosphate cycle protect cells against apoptosis induced by low doses of ionizing radiation. Radiat Res. 2000; 153(6):781–787. [PubMed: 10825753]
56. Leach JK, Black SM, Schmidt-Ullrich RK, Mikkelsen RB. Activation of constitutive nitric-oxide synthase activity is an early signaling event induced by ionizing radiation. J Biol Chem. 2002; 277(18):15400–15406. [PubMed: 11856735]
57. Criddle DN, Gillies S, Baumgartner-Wilson HK, Jaffar M, Chinje EC, Passmore S, Chvanov M, Barrow S, Gerasimenko OV, Tepikin AV, Sutton R, Petersen OH. Menadione-induced reactive oxygen species generation via redox cycling promotes apoptosis of murine pancreatic acinar cells. J Biol Chem. 2006; 281(52):40485–40492. [PubMed: 17088248]
58. Ranji M, Kanemoto S, Matsubara M, Grosso MA, Gorman JH 3rd, Gorman RC, Jaggard DL, Chance B. Fluorescence spectroscopy and imaging of myocardial apoptosis. J Biomed Opt. 2006; 11(6):064036. [PubMed: 17212559]
59. Corda S, Laplace C, Vicaut E, Duranteau J. Rapid reactive oxygen species production by mitochondria in endothelial cells exposed to tumor necrosis factor-alpha is mediated by ceramide. Am J Respir Cell Mol Biol. 2001; 24(6):762–768. [PubMed: 11415943]

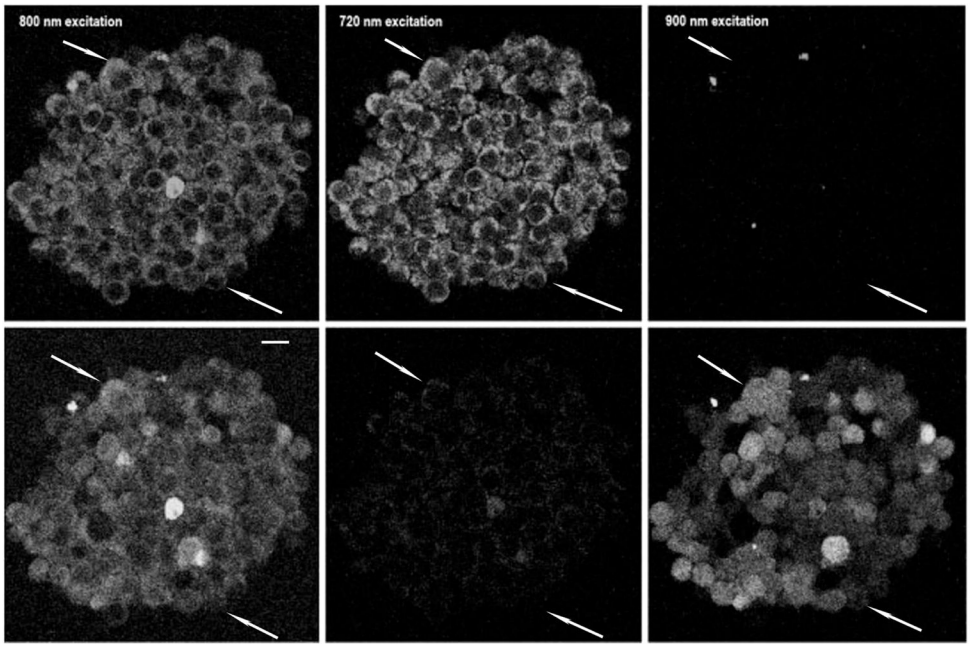

Fig. 1.

Fluorescence images of pluripotent neural spheroids at different excitation/emission settings. Fluorescence excited at 800, 720 and 900 nm (from left to right). Top row: emission isolated through 420–475 nm band filter (blue channel); Bottom row: emission isolated through 500–550 nm band filter (green channel). Arrows indicate representative cells in a spheroid: top arrow indicates a cell with high diffuse Fp fluorescence component, bottom arrow — a cell with low Fp diffuse component. Bar = 20 μm.

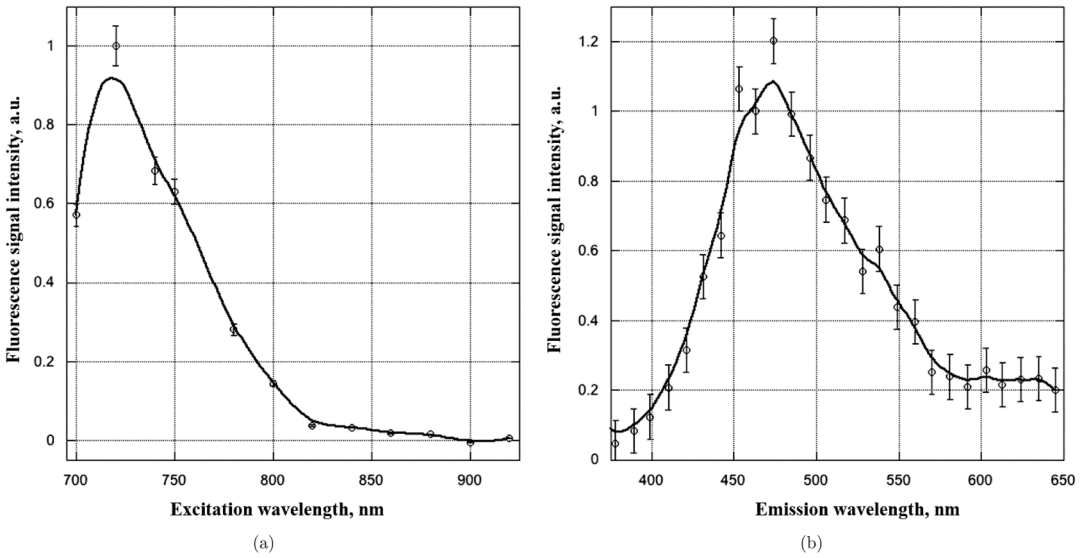

Fig. 2.

Two-photon excitation (emission set at 465 nm) and emission spectra (excitation set at 720 nm) of NAD(P)H fluorescence signal. Data were collected from cells without significant diffuse green fluorescence.

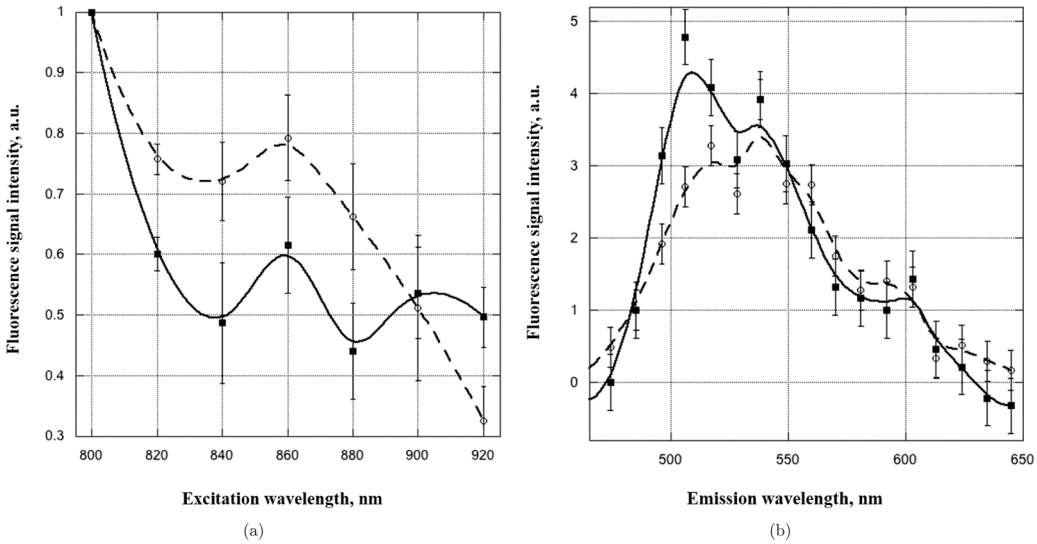

Fig. 3.

Excitation (emission set at 550 nm) and emission (excitation set at 900 nm) spectra of "green" fluorescence component (FAD+, LipDH) were measured at mitochondrial (solid line) and nuclear/cytoplasm ("diffuse") localization (broken line).

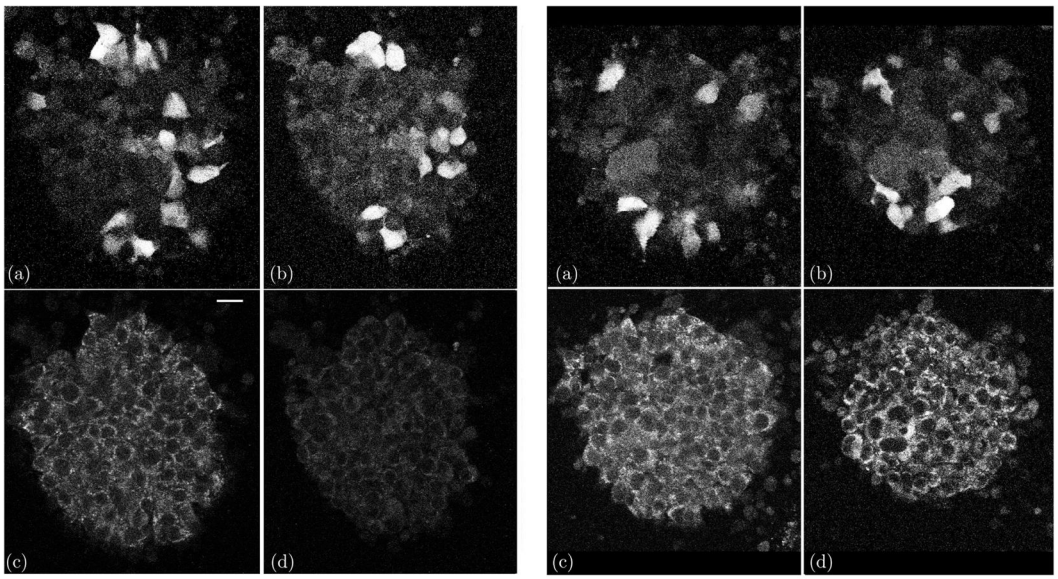

Fig. 4.

Fluorescence images of NAD(P)H and Fp after addition of Menadione (left panel) and Antimycin A (right panel). Top row: Fp fluorescence (excitation at 900 nm/emission at 500–550 nm), bottom row: NAD(P)H (excitation at 720 nm/emission 420–475 nm); (a, c) before; (b, d) −30 min after inhibitor addition. All LUTs in each row are the same. Bar = 20 μm.

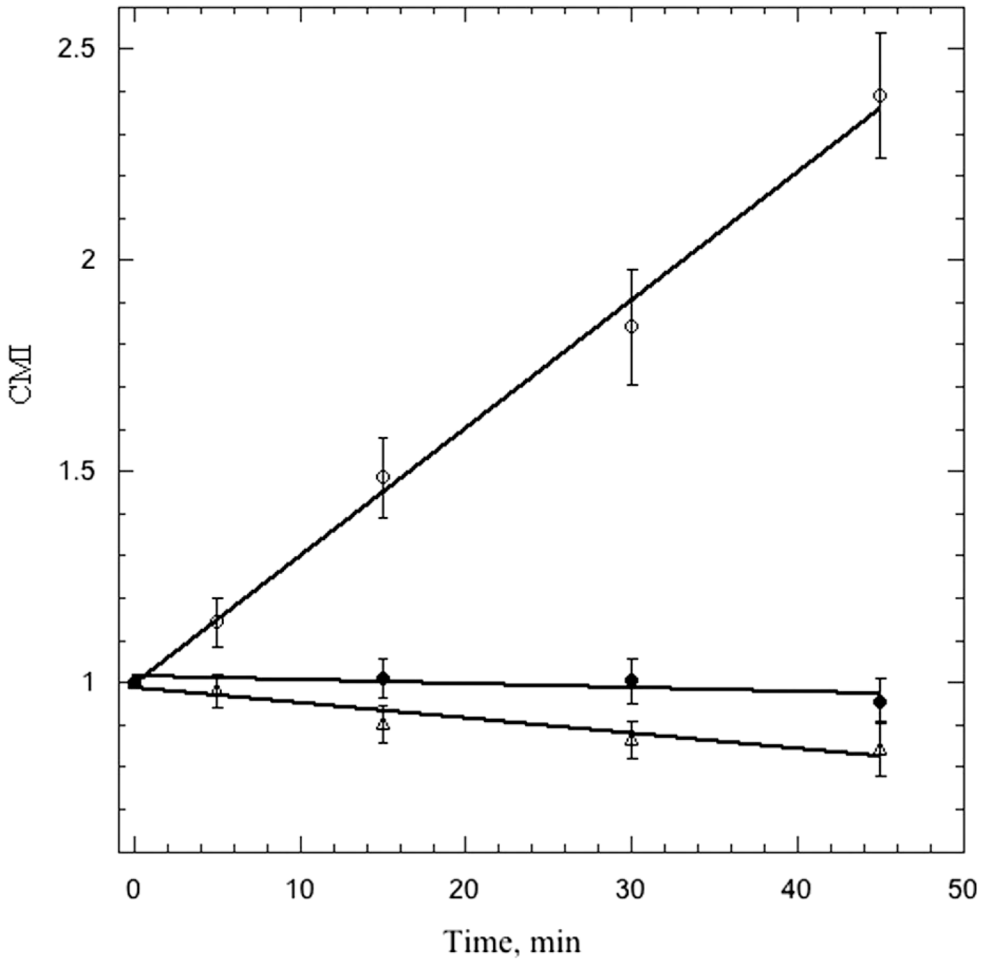

Fig. 5.

Effects of complex I (Menadione, MEN) and complex III (Antimycin A, AntA) modulators on CMI value. Ethyl alcohol was used as a negative control. Open circle, MEN; open triangle, AntA; and filled circle, EthOH. (CMI = Fp/NAD(P)H).

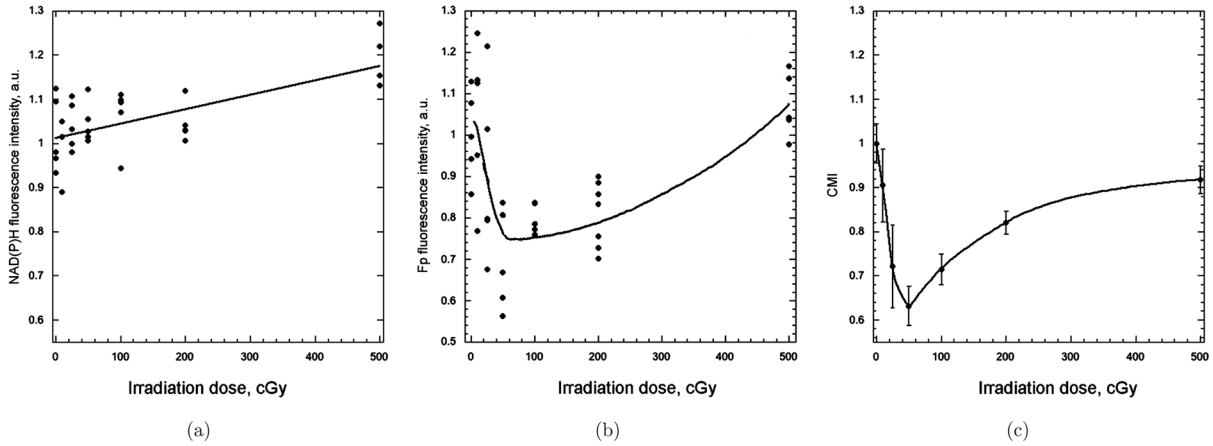

(a) (b) (c)

Fig. 6.

Effects of irradiation on cellular metabolic index CMI. (a) normalized average NAD(P)H fluorescence; (b) normalized average F_P fluorescence; (c) CMI.

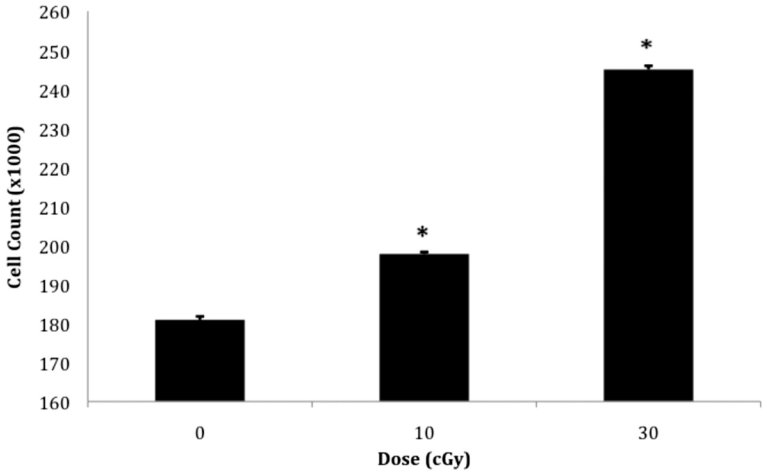

Fig. 7.

Neurospheres subjected to low-dose radiation show an increase in proliferation. Cells were seeded at 10,000/well and were allowed to grow for 4 days after irradiation. The results are highly significant (*, $P < 0.05$ ANOVA, as compared to sham-irradiated controls).